Precursor types predict the stability of neuronal branches

Joachim Fuchs[1]* and Britta J. Eickholt[1]*

[1] Charité – Universitätsmedizin Berlin, *corporate member of Freie Universität Berlin, Humboldt-Universität zu Berlin, and Berlin Institute of Health,* Institute of Molecular Biology and Biochemistry, Virchowweg 6, 10117 Berlin, Germany

* To whom correspondence should be addressed: joachim.fuchs@charite.de or britta.eickholt@charite.de

Summary statement

Branches of neurons differ in stability. We describe evidence that this stability is already defined during formation, suggesting separate branch maintenance modes initiated by distinct branch precursors.

Abstract

Branches are critical for neuron function, generating the morphological complexity required for functional networks. They emerge from different, well-described, cytoskeletal precursor structures that elongate to branches. While branches are thought to be maintained by shared cytoskeletal regulators, our data from mouse hippocampal neurons indicate that the precursor structures trigger alternative branch maintenance mechanisms with differing stabilities.

While branches originating from lamellipodia or growth cone splitting events collapse soon after formation, branches emerging from filopodia persist. Furthermore, compared to other developing neurites, axons stabilise all branches and preferentially initiate branches from filopodia. These differences explain the altered stability of branches we observe in neurons lacking the plasma membrane protein phospholipid phosphatase related protein 3 (PLPPR3/PRG2) or neurons treated with Netrin-1. Rather than altering branch stability directly, PLPPR3 and Netrin-1 boost a 'filopodia branch program' on axons, thereby indirectly initiating more long-lived branches.

In summary, we propose that studies on branching should distinguish overall stabilising effects from effects on precursor types, ideally using multifactorial statistical models as exemplified in this study.

Keywords: neuron branch stability, PRG2/PLPPR3, directed acyclic graphs (DAGs), survival analysis, filopodium, lamellipodium

Introduction

Rivers, lightnings or trees - branches are ubiquitous in both receptive and transmitting processes in nature. Their abundance ensures optimal coverage of area, balancing maximal receptivity with the shortest distance to their origin. It is no surprise that also neurons use branches to optimise their signalling efficacy in a neuronal network. The cellular mechanisms controlling this specific branching behaviour have been studied for 30 years (summarised in Kalil and Dent, 2014). Recently, branching gained attention in the setting of regenerative growth of central nerve cells (Griffin and Bradke, 2020). Strategies to improve recovery following injury to the CNS include promoting branch formation in non-injured neurons to form alternative pathways (Fink et al., 2017) or inhibiting branching in injured neurons to facilitate undisturbed elongation (Tedeschi et al., 2019).

The main drivers of the remarkable morphology of neurons, the actin and microtubule components of the cytoskeleton, participate sequentially in branch formation. Initially, F-actin structures – filopodia or lamellipodia – remodel the plasma membrane. Subsequently, de-bundling, transport, and polymerisation of microtubule arrays into the actin-enriched protrusion elongate the emerging branch. Not every branch will persist, however. Branches are maintained mainly by stabilising the microtubule cytoskeleton (Gallo, 2011; Kalil and Dent, 2014). Supporting this sequential model, F-actin regulators have been described to control branch emergence, while branch elongation requires crosslinkers between the two cytoskeletal structures, and branch maintenance is influenced predominantly by microtubule-associated proteins (Armijo-Weingart and Gallo, 2016).

Neurons establish networks by connecting selectively to specific regions and by establishing layer-specific receptive fields (Cuntz et al., 2010). Especially in long axons, this requires preventing most branching (Gibson and Ma, 2011). To circumvent the suppression of branching at specific sites, neurons rely on several extrinsic and intrinsic cues. One major regulator of branching, the PI3K/PTEN pathway, triggers F-actin accumulation and protrusion formation (Kakumoto and Nakata, 2013; Ketschek and Gallo, 2010), induces transport and local translation (Akiyama and Kamiguchi, 2010; Spillane et al., 2013), and regulates microtubule stability (Kath et al., 2018). We previously described a transmembrane protein, plasticity related gene 2/phospholipid phosphatase related protein 3

(PRG2/PLPPR3), that is able to relieve the general branch suppression by inhibiting PTEN, the negative regulator of PI3K signalling. Specifically, PLPPR3 redistributes growth towards branches by inducing filopodia formation (Brosig et al., 2019). Given that PI3K signalling is involved in multiple steps of branching, we set out to analyse the contribution of PLPPR3 to later stages, specifically to branch maintenance.

Results

Plppr3$^{-/-}$ branches are less stable

We employed phase-contrast microscopy of cultured mouse neurons from wildtype (*WT*) and *Plppr3*$^{-/-}$ hippocampus. Neurons were imaged for 24 h, at a temporal precision of 10-min intervals. In initial observations, *Plppr3*$^{-/-}$ branches appeared less stable (Movie S1, Fig. S1A). We therefore measured the lifetime of each branch as the difference between the time of initiation and, if applicable, collapse, in a blinded and randomised manner. However, such a lifetime measure depends strongly on the length of the observed time window and is extremely biased towards short lifetimes that collapse during observation. In our experiments, 40% of the branches did not collapse during the observed time window even if they persisted for hours (heavily right-censored data, Fig. 1A).

Instead of raw lifetimes we therefore quantified the risk for collapsing (the hazard ratio) using Cox proportional hazard regression, a method commonly used in clinical trials to mitigate the effects of censoring in follow-up data (Leung et al., 1997). In such survival, or time-to-event analyses, hazard ratios (HR) above 1 and decreased survival curves indicate an increased risk for branch collapse. This analysis established the *Plppr3* genotype as a predictor for branch stability (Fig. 1B&C, $HR_{Plppr3\text{-}/\text{-}}$: 1.2 (95% confidence interval: 1.1-1.3), p=0.006). Counterintuitively however, this effect is not evidence that PLPPR3 *directly* affects branch maintenance. Deeper analyses establish the effect of PLPPR3 on branch stability as secondary to its primary effect of inducing one specific branch precursor, filopodia.

Type of branch precursor predicts branch stability

During our analyses of branch stability in developing neurons, axonal branches appeared to persist longer than branches on immature dendrites (Movie S1, Fig. S1A). Supporting this, survival analyses of these branches distinguishing their neurite type (axon or immature dendrite) show a strong risk of collapse for branches on immature dendrites (Fig. 1D-F, $HR_{Neurite\ type}$=5.2 (4.6-5.9), p<0.001). This increased stability for axon branches is likely affected by mechanisms that govern stability of the

newly polarised axon shaft. Here, microtubule stability has been observed to differ in developing axons and dendrites and even contributes to initial axon specification (Witte et al., 2008). Microtubule stability in turn is regulated by distinct microtubule-binding proteins in axons (reviewed in Conde and Cáceres, 2009) and correlates well with differences in orientation and post-translational modifications of microtubules (reviewed in Janke and Magiera, 2020).

To our surprise, however, the type of F-actin based branch precursor *also* strongly influenced subsequent branch stability. We classified branches by the morphology of their precursor types (Fig. 2A) as bifurcations of the growth cone ('splitting') or as formations on the axon shaft (collateral branches) originating from thin filopodia or sheet-like lamellipodia. With many collateral branches initiating from filopodia being invaded by lamellipodia directly before branch elongation (Flynn et al., 2009; Withers and Wallace, 2020), we added a hybrid class ('mixed'). Our quantification revealed that branches originating from lamellipodia and growth cone splitting were at a high risk of collapse within a few hours (HR_{Spl}=5.0 (3.8-6.6), HR_{Lam}=4.6 (3.6-5.7), both $p<0.001$), while most branches originating from filopodia remained stable throughout the 24h imaging period (Fig. 2B-D). Mixed precursor branches were at an intermediate risk of collapse (HR_{Mix}=2.6 (2.1-3.3), $p<0.001$). While lamellipodia-associated branches appear to be stochastic "trial-and-error" branch initiations, filopodial branches may be a deterministic mode that form to stay.

Axons initiate similar numbers of branches but use different precursors than immature dendrites

Similar to previous studies (Armijo-Weingart and Gallo, 2016), neurons in our experimental setup initiate most branches as collaterals, with comparable numbers of lamellipodial, filopodial and 'mixed' precursor branches, while bifurcations are scarce (Fig. 3A, Fig. S1B). Furthermore, while the total number of branch initiation events is similar between axons and immature dendrites (Fig. 3A), the proportions of the precursor types differ drastically, with filopodia mainly dominating axon branch initiations and lamellipodia being the predominant branch precursor of immature dendrites. This difference becomes even more apparent over time, when visualising which precursor type branches originated from (Fig. 3B). Most branches on axons originate from filopodia and mixed precursors and accumulate fast, while branches on immature dendrites hardly accumulate, irrespective of the precursor type. In addition to using the most efficient precursors, axons therefore also seem to stabilise branches of all precursors.

Compared to *WT*, *Plppr3*$^{-/-}$ neurons initiate fewer branches from filopodia precursors (Fig. 3A, Fig. S1B, p=0.046), without affecting initiations from other precursor types. *Plppr3*$^{-/-}$ neurons also seem to accumulate fewer branches on axons (Fig. 3B). This is in accordance with our recent study indicating a lower number of filopodia in *Plppr3*$^{-/-}$ specifically on early polarised axons, and a lower number of

axon branches at later developmental stages. Notably, the effect sizes of filopodia density, branch density (Fig. 6 in Brosig et al., 2019) and branch initiations from filopodia (this study) are very similar. This indicates that the initial filopodia number is the main determinant of the branching defect in *Plppr3*$^{-/-}$ neurons rather than a defect in filopodia-to-branch transitions.

PLPPR3 regulates branch stability via the precursor type alone

We showed that PLPPR3-loss decreases branch stability (Fig. 1B&C) and reduces the numbers of the most efficient precursor (filopodia, Fig. S1B and Brosig et al., 2019). PLPPR3 does so preferentially on axons (Brosig et al., 2019), which themselves stabilise branches (Fig. 1E&F) and utilise more efficient precursors (Fig. 3A). With such individual but interdependent information it is difficult to distinguish whether the PLPPR3 effect on branch stability is direct, as is conceivable by inducing PI3K signalling and microtubule stability, or indirect, by regulating the number of filopodia.

This information, however, helps to generate an informed causal graph (directed acyclic graph [DAG], (Pearl, 1995), which in turn can form the basis of a multifactorial statistical analysis quantifying the contribution of the various effects. A causal graph summarising these data (Fig. 3C) assumes that both precursor and neurite type directly influence branch stability, and PLPPR3 directly influences the abundance of one precursor type. Furthermore, the neurite types differ in the distribution of precursor types. According to causal graph theory (Pearl et al., 2016), to determine in this setting whether there is a direct effect of PLPPR3 on branch stability (dotted line in Fig. 3C), an analysis has to adjust for the precursor type as well as neurite type to obtain an unbiased estimate.

When adjusting a survival analysis for the contribution of precursor and neurite type, the stability of *Plppr3*$^{-/-}$ branches is indistinguishable from WT branches both when inspecting the hazard ratio (Fig. 3D, HR=0.9 (0.8-1.1), p=0.26) and the individual survival curves of all precursor type and neurite type combinations (Fig. 3E). This still means that *Plppr3*$^{-/-}$ branches are less stable than WT (Fig. 1B&C), however there is no evidence in this dataset for a *direct* effect of PLPPR3 on branch stability. The effect of PLPPR3 on branch stability is fully explainable as an *indirect* consequence of its effect on filopodia abundance.

Branch inducing factors differ in their effect on branch stabilisation

The analyses of the presented dataset uncovered that the stability of a branch is predicted by its emergence from specific precursor types. They, furthermore, suggest that altering the precursor type composition by reducing the number of filopodia induced branches, with loss of PLPPR3, can indirectly affect branch stability. To test, whether this effect of branch precursors on branch stability

generalises to other modifications of precursor types, we induced branch formation through two independent treatments. Both guidance cues (such as Netrin-1) and growth factors (such as FGF-2) increase overall branch numbers (reviewed in Kalil and Dent, 2014). While Netrin-1 has been described to induce filopodia (Dent, 2004; Szebenyi et al., 2001; Winkle et al., 2014), FGF-2 appears to additionally involve growth cone and lamellipodial effects (Dent, 2004; Dos Santos et al., 2019; Szebenyi et al., 2001). To assess, whether these treatments can alter branch stability by their effects on precursor types, we treated wild type neurons with Netrin-1 or FGF-2 one hour before recording branching behaviour for 30 hours and analysing as described before.

The results show that both Netrin-1 and FGF-2 increased initiations (Fig. 4A, Movie S2, Fig. S2A) as well as accumulation of branches on axons, verifying successful treatment conditions. FGF-2 additionally showed strong branch inductions on immature dendrites (Fig. 4B). While Netrin-1 seemed to predominantly affect branch inductions from axonal filopodia, FGF-2 appeared to increase inductions from all precursor types without changing the overall composition of precursors (Fig. 4A&B, Fig. S2B). Interestingly, both Netrin-1 and FGF-2 affected branch stability (Fig. 4C-F). While Netrin-1 induced branches were more stable ($HR_{Netrin\text{-}1}$: 0.81, 95% CI: 0.68-0.96, p=0.018), FGF-2 treated branches were at a higher risk to collapse ($HR_{FGF\text{-}2}$: 1.21, 95% CI: 1.04-1.42, p=0.015).

Given the observed and published effects of Netrin-1 and FGF-2 on precursor types (Dent, 2004), the causal graph for this comparison is very similar to the graph describing PLPPR3-loss (Fig. 4G). As before, the graph can be used to specify a multifactorial survival analysis to estimate the effects on branch stability that are not mediated by altered precursor type compositions. Interestingly, in such a controlled survival analysis, the Netrin-1 effect on branch stability is fully explained by its effect on precursor types ($HR_{Netrin\text{-}1}$: 1.0, 95% CI: 0.87-1.2, p=0.642), as was the case for PLPPR3. In contrast, the hazard ratio for FGF-2 treated branches is not altered by accounting for precursor and neurite type ($HR_{FGF\text{-}2}$: 1.2, 95% CI: 1.01-1.4, p=0.035).

This independent dataset corroborates the importance of studying precursor types when assessing branch stability. The analysis suggests a fully explainable effect of Netrin-1 on branch stability by modifying precursor type compositions. In contrast to this, FGF-2 appears to induce a more complex phenotype on branch stability with both initiating more branches while at the same time decreasing their stability.

Discussion

Branch precursor types initiate distinct branching systems

Our analyses in hippocampal neurons highlight a strong influence of neurite type as well as precursor type on branch stability. We identified that filopodia are not the most abundant precursor, but the most efficient. Losing filopodia branches (in *Plppr3*$^{-/-}$ neurons) appears to decrease the stability of the remaining branches, while a recent study suggested that specifically losing lamellipodia trended towards increased branch stability in a sample of only three neurons (Pollitt et al., 2020). Furthermore, adding filopodia branches by Netrin-1 application, increases the stability of branches. In contrast to FGF-2, these treatments appear to shift the equilibrium of branch precursor types, without affecting the stability of branches from each individual precursor. This suggests the different precursors initiate distinct types of branches with mechanistically independent maintenance programs.

This raises the question of how the configuration of the actin cytoskeleton in the branch precursor type influences branch stability hours after the precursor structures elongate? The mechanical rigidity of parallel-bundled F-actin in filopodia and the meshwork of F-actin in lamellipodia may account for differences in branch stability, as forces generated by filopodia and lamellipodia in growth cones differ (Cojoc et al., 2007), and microtubule growth is receptive to force (Janson et al., 2003). In this respect, it could be interesting to test whether long-lived precursors are more likely to induce long-lived branches or not.

Alternatively, branch precursors may recruit different actin-microtubule crosslinkers (Dogterom and Koenderink, 2019) for microtubule capture in forming branches. Interesting candidates for filopodia-induced branches could be Septin 7 or Drebrin which both participate in initial phases of microtubule invasion and localise in filopodia (Hu et al., 2012; Ketschek et al., 2016). Alternatively, precursor types could use different mechanisms to supply fresh microtubules via severing, transport or de novo nucleation. Differential modes of branch initiation have been described for the microtubule severing-enzymes katanin and spastin (Yu et al., 2008). Most importantly, branches from different precursors can be expected to differ in the microtubule stabilising factors they recruit. Here Map7 (Tymanskyj and Ma, 2019; Tymanskyj et al., 2017), Map7D2 (Pan et al., 2019), Map6 (Tortosa et al., 2017) and the endoplasmic reticulum (Farías et al., 2019) recently emerged as fruitful candidates to either mediate precursor specific or global axon-associated effects on branch stability.

Microtubules and their binding proteins, however, can also actively modify the F-actin based branch precursors. Lamellipodial actin waves both co-occur with and require dynamic microtubules (Winans et al., 2016). The microtubule-binding proteins doublecortin (Fu et al., 2013) and Gas2L1 (Willige et al., 2019) regulate F-actin stability, altering axon branching. Reduction of Map7 induces more branch

initiations while decreasing branch stability (Tymanskyj and Ma, 2019), which might be explained by inducing more lamellipodia branches or by separate effects on microtubule stability and precursor types.

The presented results furthermore inform on commonalities and differences of axonal and dendritic branching. Both developing axons and dendrites have been described to initiate branches from all precursor types (Armijo-Weingart and Gallo, 2016; Gascon et al., 2006; Heiman and Shaham, 2010; Korobova and Svitkina, 2010). However, developing axons and dendrites differ dramatically in their growth and (unsurprisingly also) branching patterns, and treating their branching programs as identical masks important differences. For this reason, many studies assess branching in an axon- or dendrite-specific manner. While this strategy allows for detecting differences between branching mechanisms, analysing them as completely unrelated processes complicates inferences about shared parts of the physiology.

The presented multifactorial analyses suggest, that both developing axons and dendrites utilise all precursor types and that the precursor types predict branch stability on immature dendrites as well as axons. The analyses further suggest that axons predominantly initiate branches from efficient precursors like filopodia, while lamellipodia-associated initiations are more common on dendrites. This distinct composition of precursor types does, however, not fully explain the differences between axon and dendrite branch stability in both presented multifactorial analyses, indicating that distinct mechanisms on axons stabilise branches irrespective of the precursor types. Given that the developing axon seems to preferentially use efficient precursors *and* to stabilise all branches irrespective of precursors in these datasets of developing neurons, future studies on branch stabilising factors should distinguish effects on all branches from those on specific precursors.

Cell biology can benefit from multifactorial analyses informed by causal models

In addition to these biological findings, this study highlights how interpreting the effects of multiple interdependent factors *independently* can misinform the mechanistic models inferred from data, often establishing more pathways than the data accounts for. While cell biology routinely uses statistical tests to protect against false positive findings in individual experiments, the integration of evidence from multiple sources by collecting and discussing data (e.g., in scientific reviews) does not formally test their relationship. Consequentially, resulting models often contain more connections than are experimentally verified.

Our work highlights the value of quantifying the relationship of individually published links in additional, multifactorial experiments. Fortunately, statistical (multiple regression) and causal tools (DAGs, counterfactuals) have evolved considerably (Hernán and Robins, 2020; Rohrer, 2018; Suttorp et al., 2015). They are frequently employed in other fields such as epidemiology (Greenland et al., 1999) or ecology (Greenacre and Primicerio, 2013; James and McCulloch, 1990) to reduce the number of false positive links in multifactorial systems.

Our study exemplifies how multifactorial statistical analyses informed by causal graphs can advance cell biology, offering a clear benefit over unifactorial ANOVAs and t-tests, and leveraging this methodological approach has the potential to clarify the structure of biological pathways.

Acknowledgements

We thank Kerstin Schlawe, Kristin Lehmann and Beate Diemer for excellent technical assistance.

Funding

Funding was provided to BJE by Deutsche Forschungsgemeinschaft (DFG, https://www.dfg.de/) under the collaborative research centre projects SFB-958 A16 and SFB/TRR-186 A10. The funders had no role in study design, data collection and analysis, decision to publish, or preparation of the manuscript.

Competing interests

The authors declare no competing interests.

Author contributions

B.J.E. and J.F. designed the experiments, J.F. performed experiments and analysis, and B.J.E. provided supervision and funding. Both authors wrote the manuscript and revised the final version.

Material and Methods

The experimental strategies are summarised in Fig. S3, and a detailed description of each step is provided below.

Animal procedures and primary neuron culture

Mice were housed and handled according to local ethical guidelines and approved animal care protocols (under the license T0347/11, Landesamt für Gesundheit und Soziales Berlin) according to the guidelines of the animal welfare of Charité Universitätsmedizin Berlin. The mice were housed in standardised conditions under 12-hour day-night cycle with water and food available ad libitum.

The *Plppr3*$^{-/-}$ line (described in Brosig et al., 2019) is maintained in a C57Bl/6 NCrl background. Heterozygous parents were bred for primary neuron culture preparation from day 16.5 embryos. Briefly, hippocampi of homozygous littermates (wildtype or knockout) were pooled for further single cell isolation without stratifying by sex. Extracellular matrix was degraded for 15 min with 10% trypsin in HBSS (Life Technologies), washed with HBSS with 1% horse serum and Neurobasal A medium before trituration to single cells with glass pipets.

Four-well glass-bottom chamber slides (µ-Slide, Ibidi) were coated sequentially with laminin (20 mg/ml) and poly-ornithine (15 mg/ml) before plating hippocampal neurons at a density of 25.000 / cm^2 in Neurobasal A medium containing 2% B27 (Life Technologies), 1% penicillin/streptomycin (Life Technologies), 100 mM β-mercaptoethanol (Applichem) and 1% GlutaMAX (Life Technologies). Neurons were grown at 37 °C and 5% CO_2 in a humidified incubator for 48 h before starting live cell imaging. Netrin-1 (100 ng/ml, R&D Systems) and FGF-2 (20 ng/ml, PeproTech) treatments were applied in the microscope setup 1h before imaging to not mechanically disturb imaging. Each individual neuron culture was considered as an independent N. The sample size was not estimated via power analysis prior to experiments due to lack of effect size estimates for the question under study. Instead, we chose the sample size to exceed typical sample sizes in cell biological experiments.

Long-term live cell microscopy

Long-term live cell recordings were undertaken with a Nikon Eclipse Ti microscope equipped with a small stagetop as well as full incubator enclosure, to maintain cells at 37 °C (in the full incubator) and 5% CO_2 and humidity (in the stagetop) throughout the imaging session. Growing hippocampal neurons were visualised using Köhler adjusted phase contrast (Ph2) brightfield microscopy in areas of similar density across conditions using Nikon's Perfect Focus System to adjust for thermal fluctuations in focus. Three fields of view per genotype per litter were imaged for 24 h in 10-min intervals resulting in 18 movies from 6 cultures per group.

Manual classification of branch events

Prior to analysis, movies were randomised and renamed automatically using a custom R script (Randomize_folder.R, https://github.com/jo-fuchs/Microscopy_analysis_snippets/tree/master/R) to perform the analysis blind to genotypes. For each movie, the total number of cells was recorded to adjust for differences in density between cultures. At each timepoint, newly forming branches (defined as processes longer than 10 µm) were marked with a region-of-interest (ROI) overlay using ImageJ/FIJI's ROI-manager (Schindelin et al., 2012). The line colour of the ROI was encoded to represent four morphologically distinct precursor types – growth cone splitting (blue), filopodium (red), lamellipodium/actin wave (green) and a mixed type (yellow).

In a second round of analysis, branch type classifications were quality controlled and for each branching event the neurite type was recorded as: (1) on an immature *dendrite* of both polarised and non-polarised neurons or (2) on the *axon* of clearly polarised neurons, defined as the persistently longest process of a neuron. Branching events on processes with cell bodies outside of the field of view were classified as *unclear*. Additionally, the timepoint of collapse for each branch was recorded as the time at which a branch – or the originating process – completely retracted. The timepoint of collapse for branches that did not collapse during the recordings was set to the last frame and treated as censored data in subsequent analyses. All ROIs were saved and exported as comma separated value (csv) files named correspondingly to the movie.

Statistical analysis of branch initiation and lifetime

All further analysis steps were performed in R/RStudio (R Core Team, 2020) and are fully documented at https://github.com/jo-fuchs/Branch-Lifetime-PRG2. Briefly, individual branch event and cell count files were merged and unblinded (merge_data.R) before merging the cell count with the individual branching data. Further cleaning steps (clean_data.R) included converting frame counts to hours, calculating lifetime, creating a censoring indicator (whether a branch was present in the last frame) and calculating inverse probability weights (1 / time until end of movie) to correct for the higher risk of censoring for branches forming close to the end of the data acquisition.

All statistical analyses are described in the R-scripts creating the figures (Figure_1.R, Figure_2.R, Figure_3.R). Branch formations per cell (Fig. S1B and Fig. S2B) were summarised per experiment. Assumptions for linear models were tested graphically using Residual vs Fitted, Q-Q, Scale-Location and Cook's distance plots and by Levene- and Shapiro-Wilk tests on residuals. Welch's t-test was used for post-hoc pairwise comparisons. In cases of more than two comparisons, p-values were adjusted using Holm's correction.

For the branch incidence (Fig. 3A, Fig. 4A) and branch accumulation (Fig. 3B, Fig. 4B) over time, branching and collapse events were binned into 2-h slots (cumulative_branches.R). For each bin, the net "flux" of branches (formed branches minus collapsed branches) was determined stratified by neurite type, precursor type and genotype. The accumulation of branches was determined by the cumulative sum of this "flux", normalised by the number of cells the branches originated from.

Survival analyses of branch lifetimes were computed using Cox proportional hazards models including individual factors (Fig. 1B, D, Fig. 2C, Fig. 4E) or the full models presented in Fig. 3D and Fig. 4H. Assumptions were tested using Schoenfeld's test and inspecting residual plots, all models were weighted by the inverse probability weight calculated above, to account for the higher chance of censoring for branches forming close to the end of the imaging session. Final styling of the figures was performed in Adobe Illustrator 2021.

References

Akiyama, H. and Kamiguchi, H. (2010). Phosphatidylinositol 3-Kinase Facilitates Microtubule-dependent Membrane Transport for Neuronal Growth Cone Guidance. *J. Biol. Chem.* **285**, 41740–41748.

Armijo-Weingart, L. and Gallo, G. (2016). It takes a village to raise a branch: Cellular mechanisms of the initiation of axon collateral branches. *Mol. Cell. Neurosci.* **84**, 36–47.

Bodakuntla, S., Jijumon, A. S., Villablanca, C., Gonzalez-Billault, C. and Janke, C. (2019). Microtubule-Associated Proteins: Structuring the Cytoskeleton. *Trends Cell Biol.* **29**, 804–819.

Brosig, A., Fuchs, J., Ipek, F., Kroon, C., Schrötter, S., Vadhvani, M., Polyzou, A., Ledderose, J., van Diepen, M., Holzhütter, H. G., et al. (2019). The Axonal Membrane Protein PRG2 Inhibits PTEN and Directs Growth to Branches. *Cell Rep.* **29**, 2028-2040.e8.

Cojoc, D., Difato, F., Ferrari, E., Shahapure, R. B., Laishram, J., Righi, M., Di Fabrizio, E. M. and Torre, V. (2007). Properties of the Force Exerted by Filopodia and Lamellipodia and the Involvement of Cytoskeletal Components. *PLoS One* **2**, e1072.

Conde, C. and Cáceres, A. (2009). Microtubule assembly, organization and dynamics in axons and dendrites. *Nat. Rev. Neurosci.* **10**, 319–332.

Cuntz, H., Forstner, F., Borst, A. and Häusser, M. (2010). One rule to grow them all: A general theory of neuronal branching and its practical application. *PLoS Comput. Biol.* **6**,.

Dent, E. W. (2004). Netrin-1 and Semaphorin 3A Promote or Inhibit Cortical Axon Branching, Respectively, by Reorganization of the Cytoskeleton. *J. Neurosci.* **24**, 3002–3012.

Dogterom, M. and Koenderink, G. H. (2019). Actin-microtubule crosstalk in cell biology. *Nat. Rev. Mol. Cell Biol.* **20**, 38–54.

Dos Santos, J. V., Yu, R. Y., Terceros, A. and Chen, B. E. (2019). FGF receptors are required for proper axonal branch targeting in Drosophila. *Mol. Brain* **12**, 1–11.

Farías, G. G., Fréal, A., Tortosa, E., Stucchi, R., Pan, X., Portegies, S., Will, L., Altelaar, M. and Hoogenraad, C. C. (2019). Feedback-Driven Mechanisms between Microtubules and the Endoplasmic Reticulum Instruct Neuronal Polarity. *Neuron* **102**, 184-201.e8.

Fink, K. L., López-Giráldez, F., Kim, I.-J., Strittmatter, S. M. and Cafferty, W. B. J. (2017). Identification of Intrinsic Axon Growth Modulators for Intact CNS Neurons after Injury. *Cell Rep.* **18**, 2687–2701.

Flynn, K. C., Pak, C. W., Shaw, A. E., Bradke, F. and Bamburg, J. R. (2009). Growth cone-like waves transport actin and promote axonogenesis and neurite branching. *Dev. Neurobiol.* **69**, 761–779.

Fu, X., Brown, K. J., Yap, C. C., Winckler, B., Jaiswal, J. K. and Liu, J. S. (2013). Doublecortin (Dcx) Family Proteins Regulate Filamentous Actin Structure in Developing Neurons. *J. Neurosci.* **33**, 709–721.

Gallo, G. (2011). The cytoskeletal and signaling mechanisms of axon collateral branching. *Dev. Neurobiol.* **71**, 201–220.

Gascon, E., Dayer, A. G., Sauvain, M. O., Potter, G., Jenny, B., De Roo, M., Zgraggen, E., Demaurex, N., Muller, D. and Kiss, J. Z. (2006). GABA regulates dendritic growth by stabilizing lamellipodia in newly generated interneurons of the olfactory bulb. *J. Neurosci.* **26**, 12956–12966.

Gibson, D. A. and Ma, L. (2011). Developmental regulation of axon branching in the vertebrate nervous system. *Development* **138**, 183–195.

Greenacre, M. and Primicerio, R. (2013). *Multivariate Analysis of Ecological Data*.

Greenland, S., Pearl, J. and Robins, J. J. M. (1999). Causal Diagrams for Epidemiologic Research. *Epidemiology* **10**, 37–48.

Griffin, J. M. and Bradke, F. (2020). Therapeutic repair for spinal cord injury: combinatory approaches to address a multifaceted problem. *EMBO Mol. Med.* **12**, 1–29.

Heiman, M. G. and Shaham, S. (2010). Twigs into branches: how a filopodium becomes a dendrite. *Curr. Opin. Neurobiol.* **20**, 86–91.

Hernán, M. and Robins, J. (2020). *Causal Inference: What If.* Boca Raton: Chapman & Hall/CRC.

Hu, J., Bai, X., Bowen, J. R., Dolat, L., Korobova, F., Yu, W., Baas, P. W., Svitkina, T., Gallo, G. and Spiliotis, E. T. (2012). Septin-driven coordination of actin and microtubule remodeling regulates the collateral branching of axons. *Curr. Biol.* **22**, 1109–1115.

James, F. C. and McCulloch, C. E. (1990). Multivariate analysis in ecology and systematics: Panacea or Pandora's box? *Annu. Rev. Ecol. Syst.* **21**, 129–166.

Janke, C. and Magiera, M. M. (2020). The tubulin code and its role in controlling microtubule properties and functions. *Nat. Rev. Mol. Cell Biol.* **21**, 307–326.

Janson, M. E., de Dood, M. E. and Dogterom, M. (2003). Dynamic instability of microtubules is regulated by force. *J. Cell Biol.* **161**, 1029–1034.

Kakumoto, T. and Nakata, T. (2013). Optogenetic Control of PIP3: PIP3 Is Sufficient to Induce the Actin-Based Active Part of Growth Cones and Is Regulated via Endocytosis. *PLoS One* **8**, 1–17.

Kalil, K. and Dent, E. W. (2014). Branch management: mechanisms of axon branching in the developing vertebrate CNS. *Nat. Rev. Neurosci.* **15**, 7–18.

Kath, C., Goni-Oliver, P., Müller, R., Schultz, C., Haucke, V., Eickholt, B. and Schmoranzer, J. (2018). PTEN suppresses axon outgrowth by downregulating the level of detyrosinated microtubules. *PLoS One* **13**, 1–18.

Ketschek, A. and Gallo, G. (2010). Nerve growth factor induces axonal filopodia through localized microdomains of phosphoinositide 3-kinase activity that drive the formation of cytoskeletal precursors to filopodia. *J. Neurosci.* **30**, 12185–12197.

Ketschek, A., Spillane, M., Dun, X. P., Hardy, H., Chilton, J. and Gallo, G. (2016). Drebrin coordinates the actin and microtubule cytoskeleton during the initiation of axon collateral branches. *Dev. Neurobiol.* 1092–1110.

Korobova, F. and Svitkina, T. (2010). Molecular Architecture of Synaptic Actin Cytoskeleton in Hippocampal Neurons Reveals a Mechanism of Dendritic Spine Morphogenesis. *Mol. Biol. Cell* **21**, 165–176.

Leung, K. M., Elashoff, R. M. and Afifi, A. A. (1997). Censoring issues in survival analysis. *Annu. Rev. Public Health* **18**, 83–104.

Pan, X., Cao, Y., Stucchi, R., Hooikaas, P. J., Portegies, S., Will, L., Martin, M., Akhmanova, A., Harterink, M. and Hoogenraad, C. C. (2019). MAP7D2 Localizes to the Proximal Axon and Locally Promotes Kinesin-1-Mediated Cargo Transport into the Axon. *Cell Rep.* **26**, 1988-1999.e6.

Pearl, J. (1995). Causal diagrams for empirical research. *Biometrika* **82**, 669–688.

Pearl, J., Glymour, M. and Jewell, N. P. (2016). *Causal Inference in Statistics: A Primer*. Chichester, England: John Wiley & Sons, Inc.

Pollitt, S. L., Myers, K. R., Yoo, J. and Zheng, J. Q. (2020). LIM and SH3 protein 1 localizes to the leading edge of protruding lamellipodia and regulates axon development. *Mol. Biol. Cell* **31**, 2718–2732.

R Core Team (2020). R: A language and environment for statistical computing. *R Found. Stat. Comput. Vienna, Austria*.

Rohrer, J. M. (2018). Thinking Clearly About Correlations and Causation: Graphical Causal Models for Observational Data. *Adv. Methods Pract. Psychol. Sci.* **1**, 27–42.

Schindelin, J., Arganda-Carreras, I., Frise, E., Kaynig, V., Longair, M., Pietzsch, T., Preibisch, S., Rueden, C., Saalfeld, S., Schmid, B., et al. (2012). Fiji: an open-source platform for biological-image analysis. *Nat. Methods* **9**, 676–682.

Spillane, M., Ketschek, A., Merianda, T. T., Twiss, J. L. and Gallo, G. (2013). Mitochondria Coordinate Sites of Axon Branching through Localized Intra-axonal Protein Synthesis. *Cell Rep.* **5**, 1564–1575.

Suttorp, M. M., Siegerink, B., Jager, K. J., Zoccali, C. and Dekker, F. W. (2015). Graphical presentation of confounding in directed acyclic graphs. *Nephrol. Dial. Transplant.* **30**, 1418–1423.

Szebenyi, G., Dent, E. W., Callaway, J. L., Seys, C., Lueth, H. and Kalil, K. (2001). Fibroblast growth factor-2 promotes axon branching of cortical neurons by influencing morphology and behavior of the primary growth cone. *J. Neurosci.* **21**, 3932–3941.

Tedeschi, A., Dupraz, S., Curcio, M., Laskowski, C. J., Schaffran, B., Flynn, K. C., Santos, T. E., Stern, S., Hilton, B. J., Larson, M. J. E., et al. (2019). ADF/Cofilin-Mediated Actin Turnover Promotes Axon Regeneration in the Adult CNS. *Neuron* **103**, 1073-1085.e6.

Tortosa, E., Adolfs, Y., Fukata, M., Pasterkamp, R. J., Kapitein, L. C. and Hoogenraad, C. C. (2017). Dynamic Palmitoylation Targets MAP6 to the Axon to Promote Microtubule Stabilization during Neuronal Polarization. *Neuron* **94**, 809-825.e7.

Tymanskyj, S. R. and Ma, L. (2019). MAP7 Prevents Axonal Branch Retraction by Creating a Stable Microtubule Boundary to Rescue Polymerization. *J. Neurosci.* **39**, 7118–7131.

Tymanskyj, S. R., Yang, B., Falnikar, A., Lepore, A. C. and Ma, L. (2017). MAP7 regulates axon collateral branch development in dorsal root ganglion neurons. *J. Neurosci.* **37**, 1648–1661.

Willige, D., Hummel, J. J., Alkemade, C., Kahn, O. I., Au, F. K., Qi, R. Z., Dogterom, M., Koenderink, G. H., Hoogenraad, C. C. and Akhmanova, A. (2019). Cytolinker Gas2L1 regulates axon morphology through microtubule-modulated actin stabilization. *EMBO Rep.* **20**, 1–20.

Winans, A. M., Collins, S. R. and Meyer, T. (2016). Waves of actin and microtubule polymerization drive microtubule-based transport and neurite growth before single axon formation. *Elife* **5**, 1–22.

Winkle, C. C., McClain, L. M., Valtschanoff, J. G., Park, C. S., Maglione, C. and Gupton, S. L. (2014). A novel netrin-1-sensitive mechanism promotes local SNARE-mediated exocytosis during axon branching. *J. Cell Biol.* **205**, 217–232.

Withers, G. S. and Wallace, C. S. (2020). Transient lamellipodia predict sites of dendritic branch formation in hippocampal neurons. *Cell Tissue Res.*

Witte, H., Neukirchen, D. and Bradke, F. (2008). Microtubule stabilization specifies initial neuronal polarization. *J. Cell Biol.* **180**, 619–632.

Yu, W., Qiang, L., Solowska, J. M., Karabay, A., Korulu, S. and Baas, P. W. (2008). The Microtubule-severing Proteins Spastin and Katanin Participate Differently in the Formation of Axonal Branches. *Mol. Biol. Cell* **19**, 1485–1498.

Figures

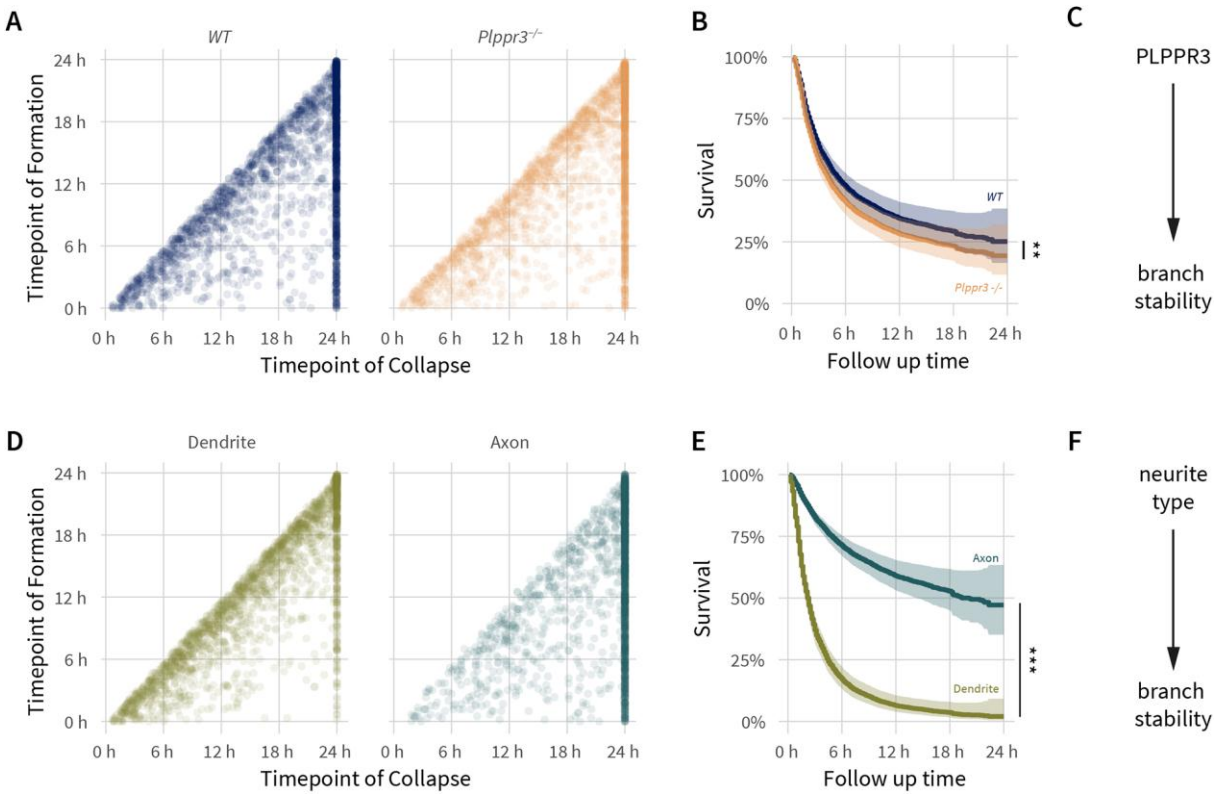

Fig. 1: Individual effects of PLPPR3 and neurite type on neuronal branch stability.

(A) Scatterplot of timepoint of formation versus collapse for individual branches shows strong right-censoring of the data. (B) Correcting for censoring-bias using survival analysis reveals a small effect of *Plppr3*-loss on branch lifetime. (C) Causal graph highlighting the connection of the *Plppr3*-genotype to branch stability. (D) Scatterplot of timepoint of formation versus collapse for individual branches shows strong enrichment of non-collapsed branches in the axonal fraction. (E) Survival analysis shows a strong effect of the neurite type on branch stability in both *WT* and *Plppr3*$^{-/-}$. (F) Causal graph highlighting the connection of the neurite type to branch stability. n_{Ind}=2317 (*WT*) & 2165 (*Plppr3*$^{-/-}$), n_{Exp}=6 (six independent cultures), transparent ribbons show 95% confidence intervals in survival curves. Survival analyses were analysed with Cox proportional hazards regression. ** p<0.01, *** p<0.001

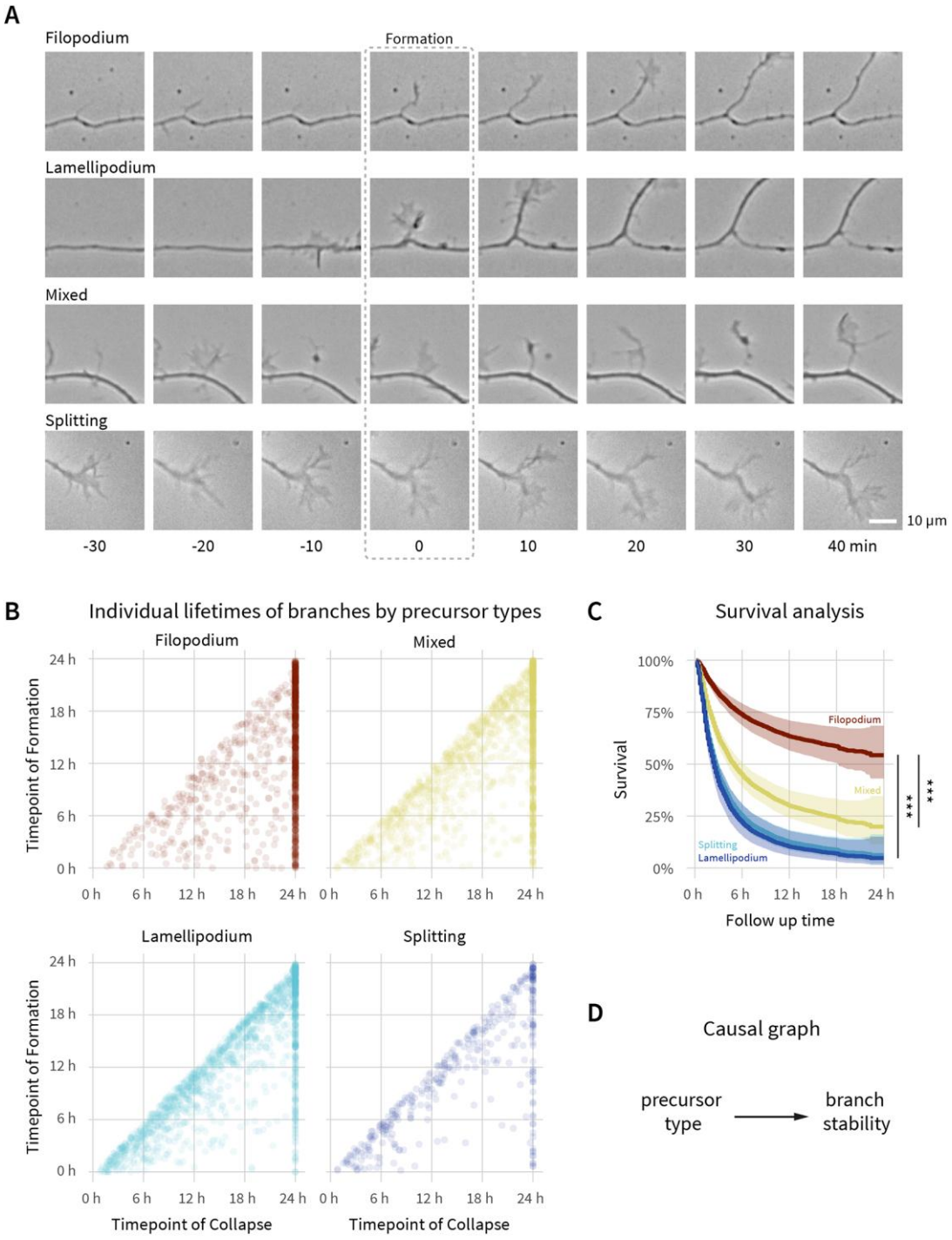

Fig. 2: Morphologically distinct branch precursor types affect branch stability.

(A) Example time series of branch precursor types. 0 indicates the timepoint of branch formation. (B) Scatterplot of timepoint of formation versus collapse for individual branches shows strong right-censoring of filopodia-associated branches when compared to other branch precursors. (C) Survival analysis shows the strong effect of the branch precursor type on stability in both *WT* and *Plppr3*$^{-/-}$, with filopodia initiating the most stable branches. (D) Causal graph highlighting connection of precursor type to branch stability. n_{Ind}=2317 (*WT*) & 2165 (*Plppr3*$^{-/-}$), n_{Exp}=6 (six independent cultures), transparent ribbons show 95% confidence intervals in survival curves. Survival analyses were analysed with Cox proportional hazards regression. *** p<0.001.

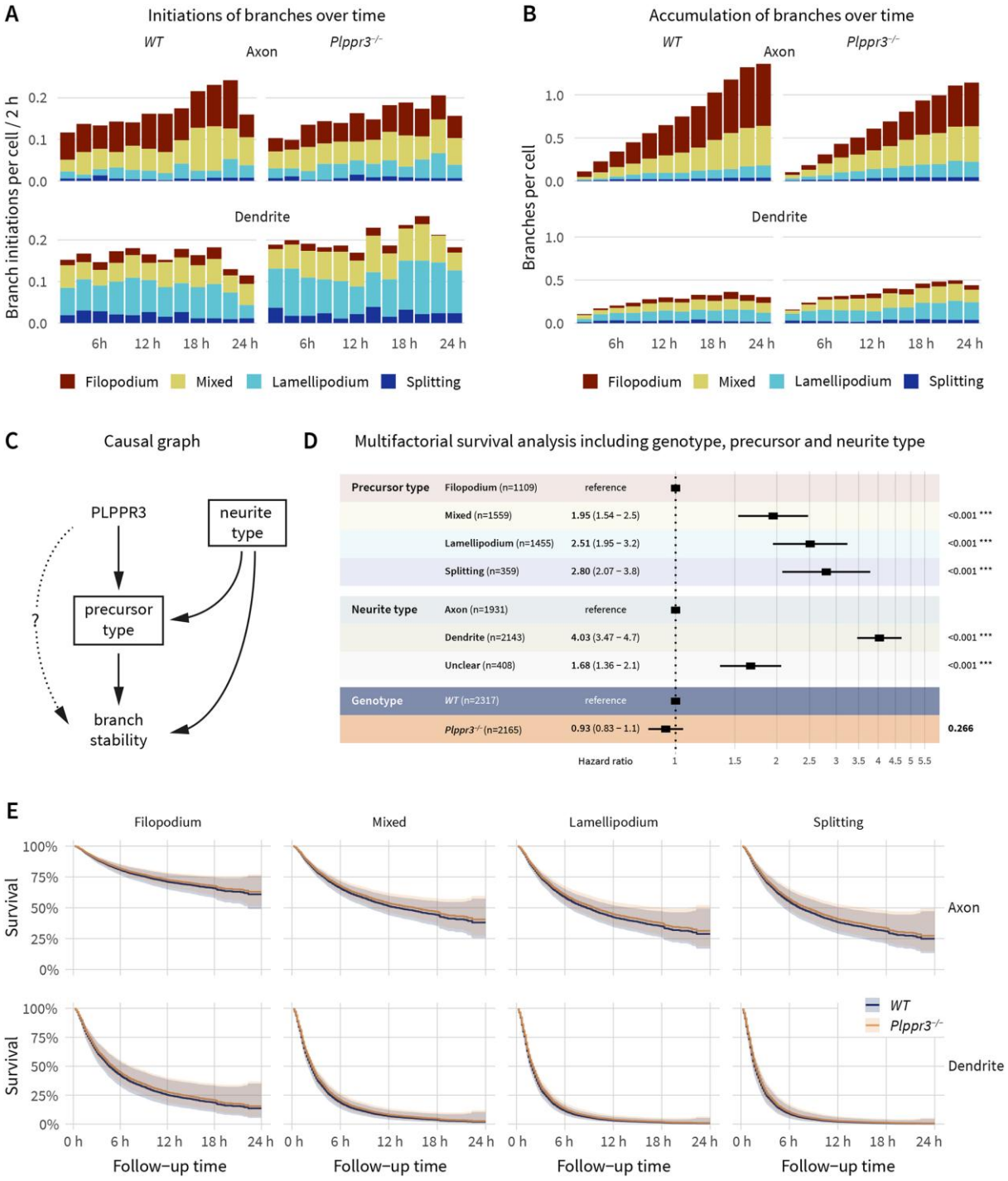

Fig. 3: Combined influences on branch stability

(A) Distribution of branch forming events over time, colour-coded by precursor type, according to neurite type as well as genotype. Timepoints are binned in 2h windows. Note the similar overall number of branch initiations but different composition of precursor types between axons and immature dendrites. (B) Branches per cell present over time, colour-coded by precursor type, according to neurite type as well as genotype. Note the increased branch accumulation on axons vs immature dendrites and the different precursor composition between branch initiations (A) and accumulating branches (B). Bin size 2h. (C) Directed acyclic graph aggregating the information from Fig 1C, 1F, 2D, 3A and Fig S1B. According to causal graph theory, to quantify a direct effect of PLPPR3

on branch stability, a multifactorial analysis has to adjust for precursor type as well as neurite type (indicated by squares). (D & E) Forest plot and survival curves of a Cox proportional hazard analysis of *WT* vs. *Plppr3*$^{-/-}$ branches including neurite type as well as precursor types as covariates demonstrates no direct effect of PLPPR3 on branch stability. Boxes in (D) indicate the hazard ratio, lines indicate the 95% confidence interval. n_{Ind}=2317 (*WT*) & 2165 (*Plppr3*$^{-/-}$), n_{Exp}=6. The opaque ribbons in (E) show the 95% confidence interval of the survival curves. *** p<0.001.

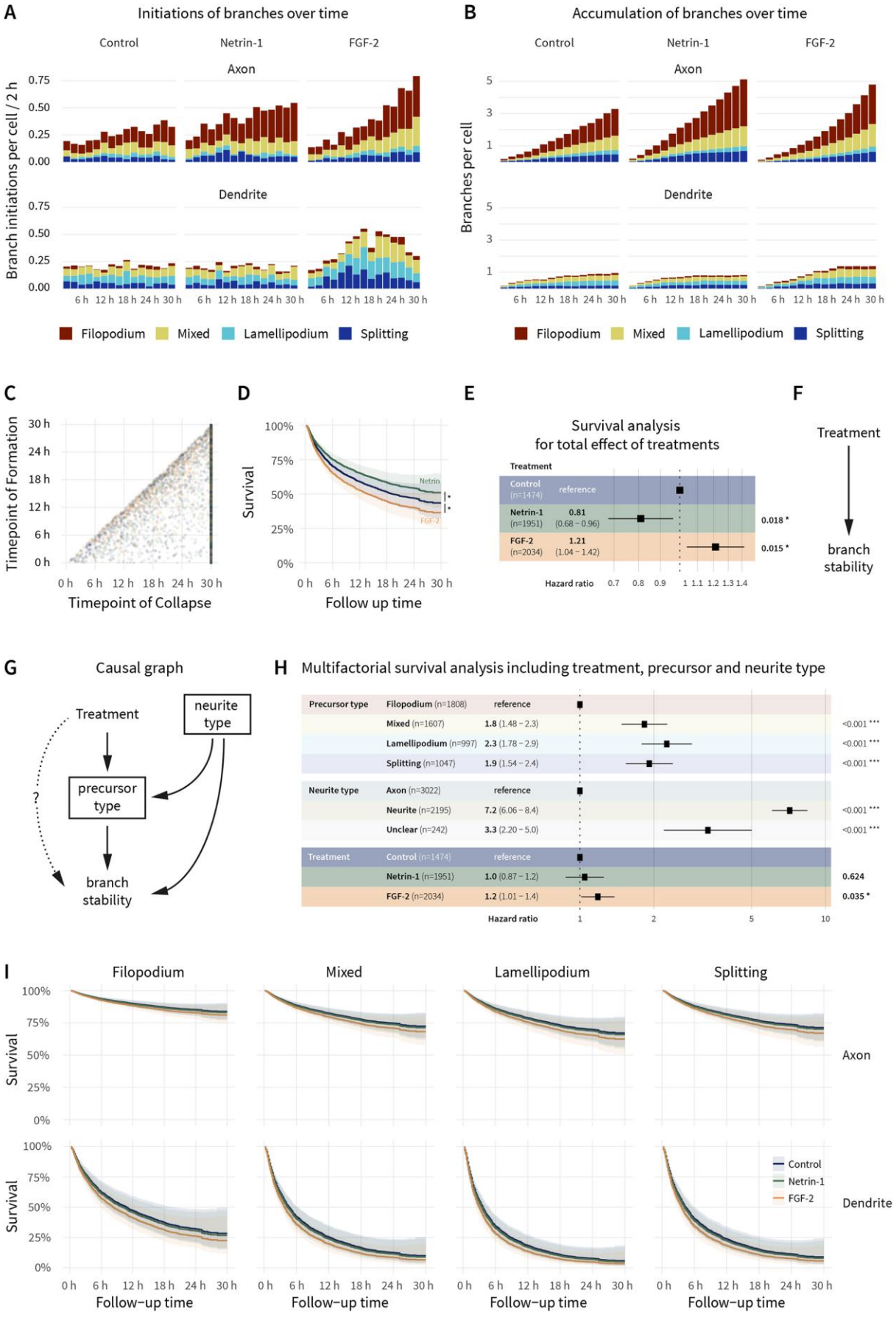

Fig. 4: Netrin-1 increases branch stability via the precursor type, FGF-2 decreases branch stability in addition to the precursor type

(A) Distribution of branch forming events over time, colour-coded by precursor type, according to neurite type as well as treatment. Note the effects of FGF-2 on both axons and dendrites and the overall increase in branch inductions over time. Bin size 2 h. (B) Branches per cell present over time, colour-coded by precursor type, according to neurite type as well as treatment. Note the increased branch accumulation after Netrin-1 and FGF-2 treatments. (C) Scatterplot of timepoint of formation versus collapse for individual branches shows strong right-censoring of the data even after 30 h. (D & E) Correcting for censoring-bias using survival analysis reveals small but opposite effects of Netrin-1 and FGF-2 on branch stability. Boxes in panel (D) indicate hazard ratio, lines indicate 95% CI. Survival analyses were analysed with Cox proportional hazards regression. (F) Causal graph highlighting the total effects of treatments on branch stability. (G) Directed acyclic graph for testing precursor type independent effects of the treatments on branch stability. As in the previous experiment, a multifactorial analysis has to account for precursor type as well as neurite type (indicated by squares). (H) Forest plot of a Cox proportional hazard analysis of control vs. Netrin-1 or FGF-2 treated branches including neurite type as well as precursor types as covariates demonstrates no direct effect of Netrin-1 on branch stability but more complex effects of FGF-2. Note how the hazard ratio of Netrin changes compared to the analysis in I while the hazard ratio of FGF-2 is not affected. Boxes indicate hazard ratio, lines indicate 95% CI. (I) Survival curves of this analysis. Note the near perfect match of Control and Netrin-1 survival curves and the slight difference of the FGF-2 curve in panel (I). n_{Ind}=1474 (Control), 1951 (Netrin-1), 2034 (FGF.2) n_{Exp}=3. The opaque ribbons in (D & I) show the 95% confidence interval of the survival curves. * $p<0.05$, *** $p<0.001$

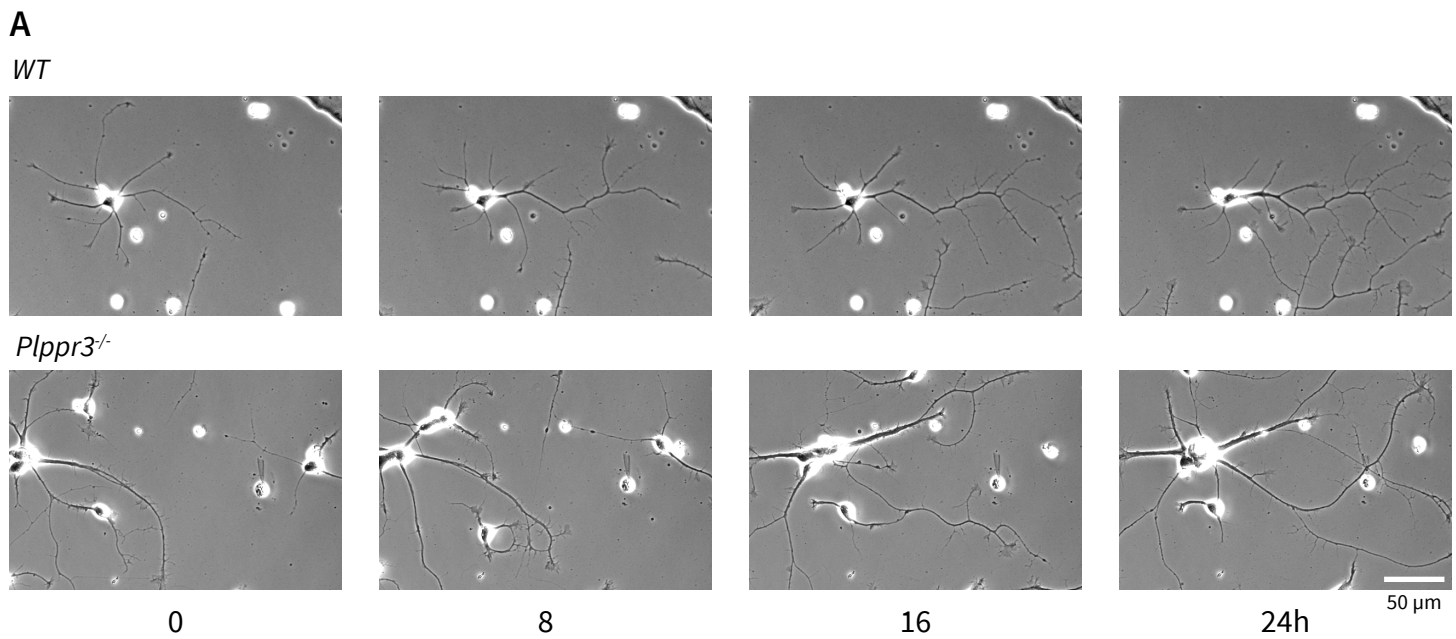

Fig. S1. Branching in *wildtype* versus *Plppr3*$^{-/-}$ neurons.
(A) Timeseries of Movie S1 of *WT* and *Plppr3*$^{-/-}$ mouse hippocampal neurons. Note the higher increased dynamics of branches in *Plppr3*$^{-/-}$. (B) Total branch formations per cell over 24 h, originating from different precursor types and genotype. *Plppr3*$^{-/-}$ neurons initiate fewer branches from filopodia. Error bars in (B) indicate s.e.m., data were tested with one-way ANOVA and post-hoc Welch's t-test with Holm correction for multiple testing. * $p < 0.05$.

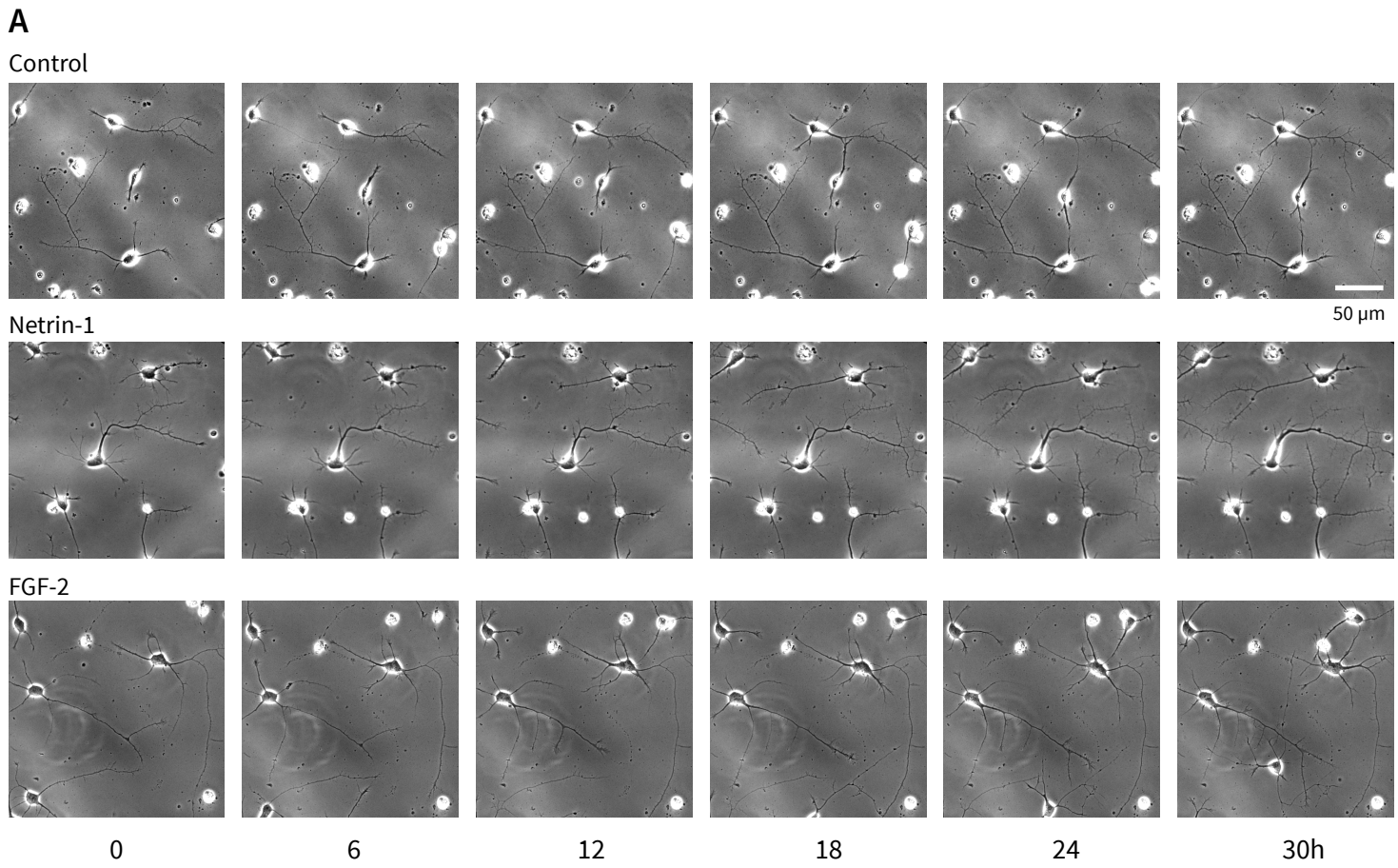

Fig. S2. Branching inducing treatments Netrin-1 and FGF-2

(A) Timeseries of Movie S2 of control, Netrin-1- and FGF-2 treated mouse hippocampal neurons. Note the increased branching from filopodia after Netrin-1, and the increased branch dynamics after FGF-2 treatment (B) Total branch formations per cell over 30 h, originating from different precursor types segregated by treatments. Netrin-1 treated neurons trend to initiate more branches from filopodia, FGF-2 treated neurons trend to initiate more branches from all precursors. While these effects are in line with published evidence on Netrin-1 and FGF-2 (Dent, 2004), they were not statistically detectable at three experiments and should be verified in future confirmatory studies. Error bars in (B) indicate s.e.m., data were tested with one-way ANOVA and post-hoc Welch's t-test with Holm correction for multiple testing.

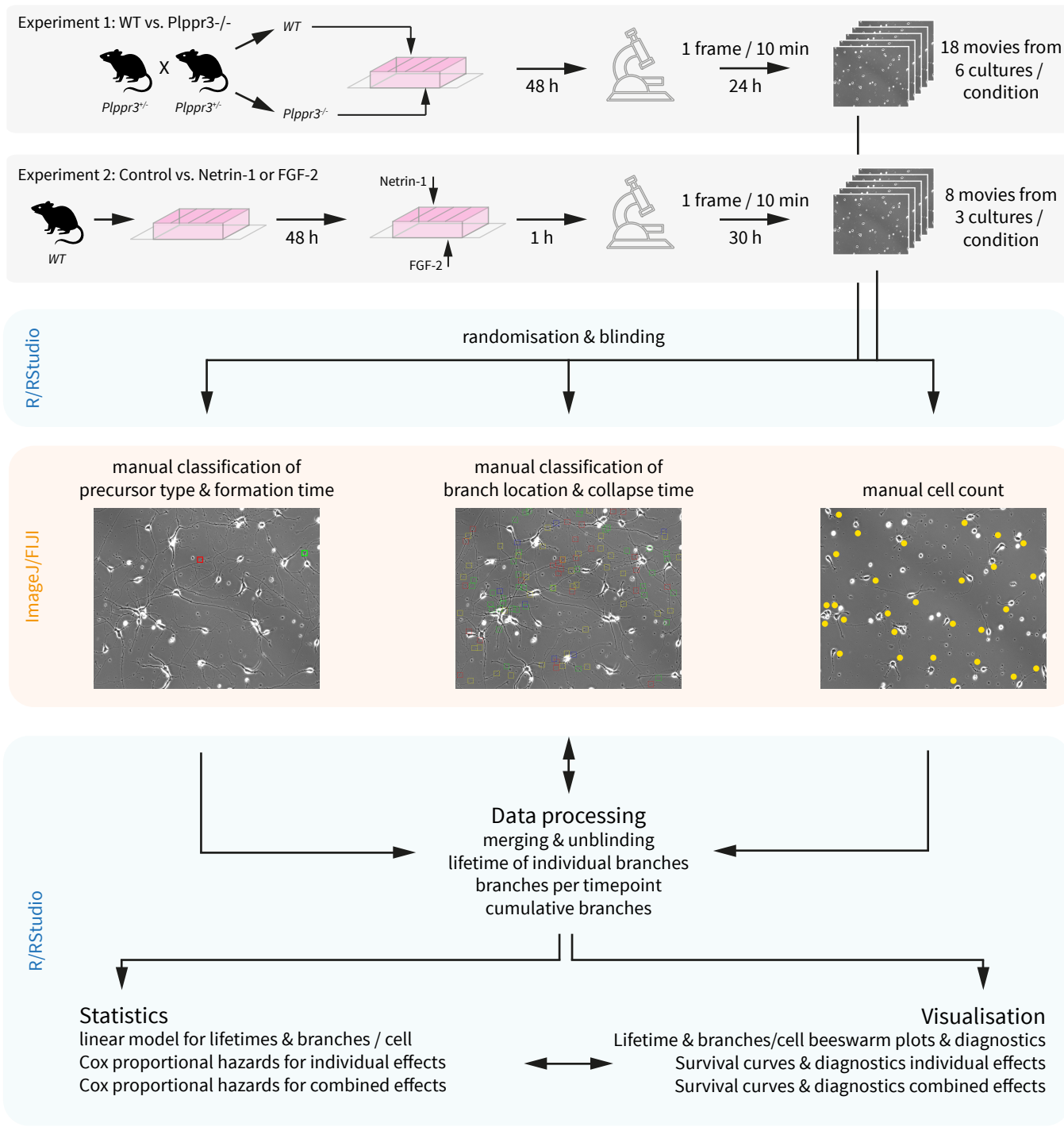

Fig. S3. Workflow of experiments and analysis

Experiment 1: *Plppr3*$^{-/-}$ and *WT* hippocampal neuron cultures were prepared from littermates of heterozygous *Plppr3*$^{+/-}$ mice and grown on poly-ornithine & laminin-coated 4-well chamber slides for 48 h. Experiment 2: *WT* hippocampal neuron cultures were grown on poly-ornithine & laminin-coated 4-well chamber slides for 48 h before treating wells with 100 ng/ml Netrin-1, 20 ng/ml FGF-2, or an equal volume of medium for 1 hour before acquiring images. Branching was imaged using phase contrast (Ph2) light microscopy for 24 h (Experiment 1) or 30 h (Experiment 2) with an interval of 10 min. Before manual branch classification in FIJI, each experiment was randomised and blinded to reduce bias in quantification. The analysis consisted of a three-step process, first classifying formation time and precursor type followed by collapse time and neurite type of individual branches. Finally, cells per movie were counted to normalise differences in density between cultures. All subsequent steps of the analysis were performed using R/RStudio and are fully documented at https://github.com/jofuchs/Branch-Lifetime-PRG2.

Table S1. Key resources

Reagent or Resource	Source	Identifier
Deposited data		
Individual branch classifications and lifetimes (Individual_branches.csv)	This paper	https://github.com/jo-fuchs/Branch-Lifetime-PRG2
Cells number and genotypes per movie in analysis (Cells.csv)	This paper	https://github.com/jo-fuchs/Branch-Lifetime-PRG2
Experimental Models: Organisms/Strains		
C57Bl/6 NCrl *Plppr3*$^{-/-}$ mice	Brosig et al., 2019	-
C57Bl/6 NCrl mice	Charles River	Cat# CRL:027 RRID: IMSR_CRL:027)
Chemicals		
Netrin-1	R&D Systems	Cat#: 1109-N1
FGF-2 (FGF-basic)	PeproTech	Cat#: AF-100-18B
Software and Algorithms		
Full analysis scripts in R	This paper	https://github.com/jo-fuchs/Branch-Lifetime-PRG2
FIJI	Schindelin et al., 2012	https://imagej.net/Fiji
R	R Core Team, 2020	http://www.r-project.org/index.html

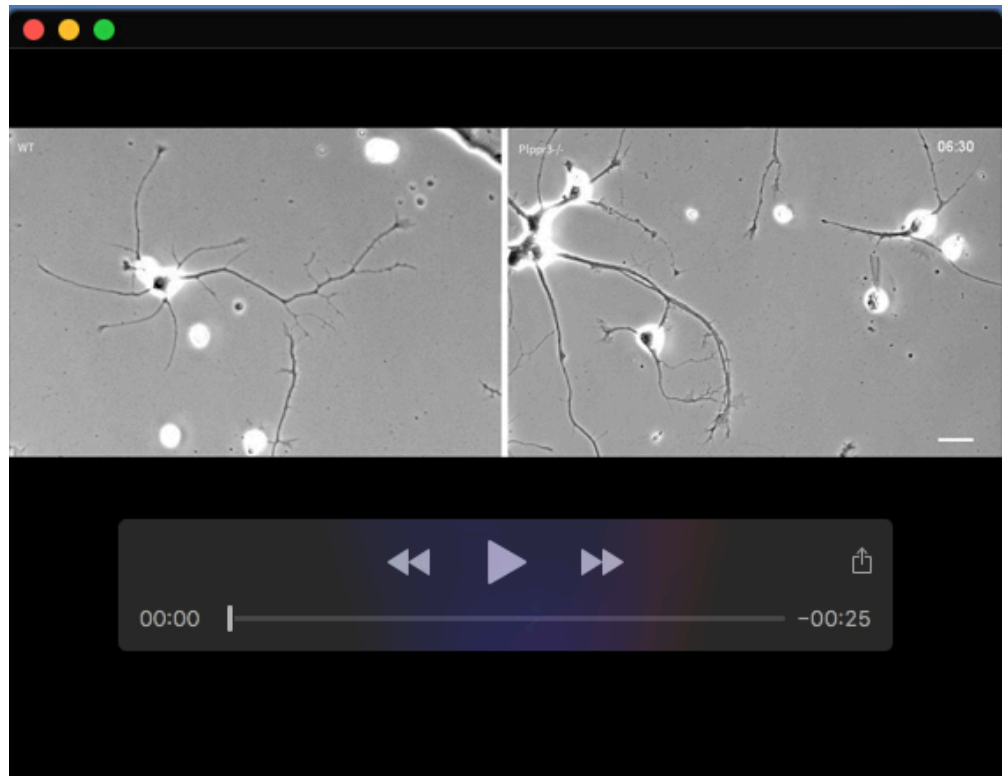

Movie 1. Branching in primary wildtype versus *Plppr3*$^{-/-}$ mouse hippocampal neurons.
24-hour phase-contrast time-lapse movie with 10 min intervals starting at day in vitro 2. Scale: 20 µm.

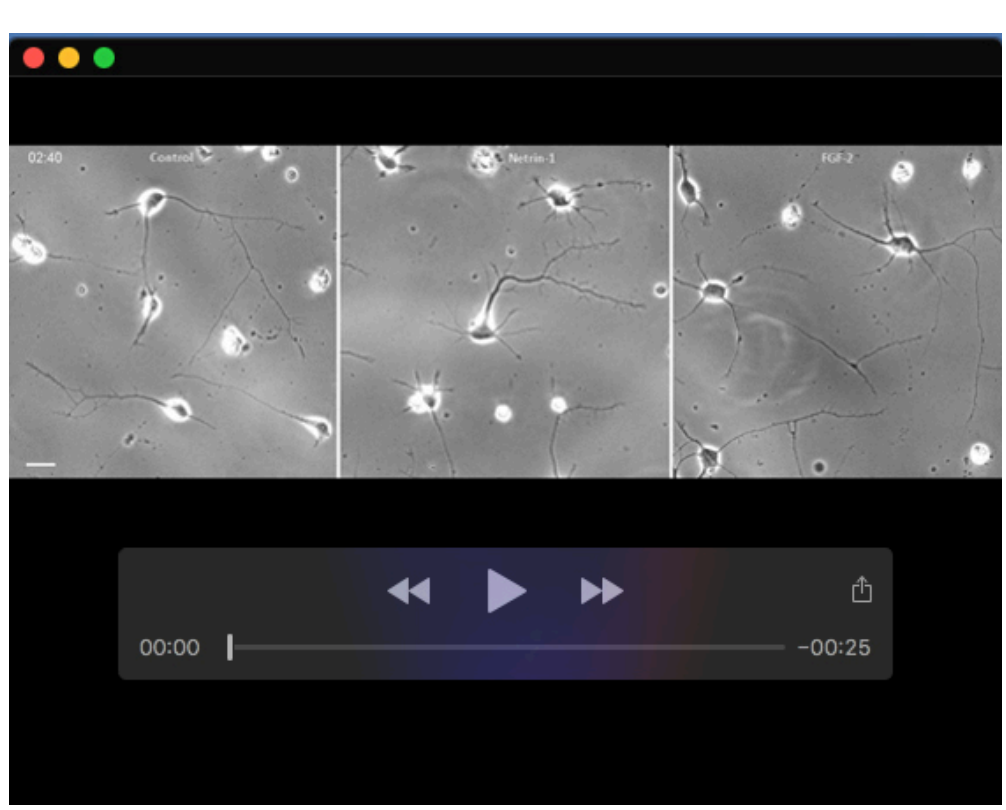

Movie 2. Branching in primary wildtype mouse hippocampal neurons after Netrin-1 or FGF-2 stimulation. 30-hour phase-contrast time-lapse movie with 10 min intervals starting at day in vitro 2. Treatments were applied one hour before imaging. Netrin-1: 100 ng/ml, FGF-2: 20 ng/ml. Scale: 20 µm.